Title

Multiple sulfur isotope constraints on the modern sulfur cycle

Permalink

https://escholarship.org/uc/item/8b47c2tj

Authors

Tostevin, Rosalie
Turchyn, Alexandra V
Farquhar, James
et al.

Publication Date

2014-06-01

DOI

10.1016/j.epsl.2014.03.057

Peer reviewed

Multiple sulfur isotope constraints on the modern sulfur cycle

Rosalie Tostevin [a,*], Alexandra V. Turchyn [b], James Farquhar [c], David T. Johnston [d], Daniel L. Eldridge [c], James K.B. Bishop [e], Matthew McIlvin [f]

[a] Department of Earth Sciences, University College London, Gower Street, London, WC1E 6BT, UK
[b] Department of Earth Sciences, University of Cambridge, Downing Street, Cambridge, CB2 3EQ, UK
[c] Department of Geology and Earth Systems Science Interdisciplinary Center, University of Maryland, College Park, MD 20742, USA
[d] Department of Earth and Planetary Sciences, Harvard University, Cambridge, MA 02138, USA
[e] Department of Earth and Planetary Science, University of California, Berkeley, Berkeley, CA 94720-4767, USA
[f] Marine Chemistry and Geochemistry, Woods Hole Oceanographic Institution, Woods Hole, MA 02543, USA

ABSTRACT

We present 28 multiple sulfur isotope measurements of seawater sulfate ($\delta^{34}S_{SO_4}$ and $\Delta^{33}S_{SO_4}$) from the modern ocean over a range of water depths and sites along the eastern margin of the Pacific Ocean. The average measured $\delta^{34}S_{SO_4}$ is 21.24‰ (± 0.88‰, 2σ) with a calculated $\Delta^{33}S_{SO_4}$ of $+0.050$‰ (± 0.014‰, 2σ). With these values, we use a box-model to place constraints on the gross fraction of pyrite burial in modern sediments. This model presents an improvement on previous estimates of the global pyrite burial flux because it does not rely on the assumed value of $\delta^{34}S_{pyrite}$, which is poorly constrained, but instead uses new information about the relationship between $\delta^{34}S$ and $\delta^{33}S$ in global marine sulfate. Our calculations indicate that the pyrite burial flux from the modern ocean is between 10% and 45% of the total sulfur lost from the oceans, with a more probable range between 20% and 35%.

© 2014 The Authors. Published by Elsevier B.V. This is an open access article under the CC BY license (http://creativecommons.org/licenses/by/3.0/).

1. Introduction

Sulfate is the second most abundant anion in the oceans and has a residence time of 10–20 million years, which far exceeds the mixing time of the ocean (Paytan et al., 2004). As a result, the concentration of sulfate, 28 mM, and its sulfur isotope composition should not vary among or within ocean basins. Sulfate is supplied to the ocean through rivers and removed during pyrite and evaporite mineral deposition and during hydrothermal alteration of the ocean crust (Kaplan, 1983; Krouse, 1980). Sulfate is respired during dissimilatory sulfate reduction by sulfate reducing microbes in anoxic sediments (Jørgensen, 1982). The sulfide produced during this sulfate reduction can either be buried as pyrite and enter the geologic record or be returned to the marine sulfate pool via abiotic or biotic sulfide oxidation.

The $\delta^{34}S$ of modern ocean sulfate is spatially homogeneous, and its value reflects the sources and sinks of sulfate to the ocean; the $\delta^{34}S$ of marine sulfate is particularly sensitive to the $\delta^{34}S$ of river input, the $\delta^{34}S$ associated with pyrite burial, and the flux of the buried pyrite sink (Berner and Canfield, 1989;

Garrels and Lerman, 1981, 1984). The $\delta^{34}S$ of river input reflects the minerals being weathered, and is typically thought to be between 5 and 15‰ (Canfield, 2004, 2013; Holser et al., 1988; Kurtz et al., 2003). The traditional accepted value for the $\delta^{34}S$ of marine sulfate is 20.3‰, with a typical uncertainty of ± 0.8‰ (2σ) (from the reproducibility of the international marine sulfate standard, IAEA NBS127). Rees (1978) later demonstrated that there is a slight bias towards lower $\delta^{34}S$ values when sulfur isotopes are measured via combustion to sulfur dioxide and redefined the seawater value closer to 20.6‰. This $\delta^{34}S$ of marine sulfate is elevated over the $\delta^{34}S$ of the global river input because of the preferential burial of ^{32}S rich pyrite in marine sediments.

The sulfur isotopic composition of pyrite is controlled by sulfate reducing microorganisms as well as organisms that metabolize sulfur compounds at oxidation states intermediate between sulfide and sulfate. A wide phylogenetic range of microorganisms have been studied both *in situ* and in the laboratory setting to assess their sulfur isotope partitioning (Canfield et al., 2010; Chambers and Trudinger, 1979; Johnston et al., 2005, 2007; Kaplan and Rittenberg, 1964; Leavitt et al., 2013; Sim et al., 2011; Zerkle et al., 2009). These studies have shown that the sulfur isotope fractionation varies as a function of the metabolic make-up of the microbial community and the growth conditions (e.g. pressure, temperature, organic carbon availability, sulfate concentrations and

---

type of electron donors). A wide range of sulfur isotope fractionation can result from microbial sulfate reduction by even a single species of bacteria (Leavitt et al., 2013; Sim et al., 2011), and large sulfur isotope fractionations have also been recorded in natural populations of sulfate reducers (Canfield et al., 2010). When a range of metabolisms cohabitate in natural environments, the result is a mix of $\delta^{34}S$ signatures that often offset one another. As a result, pyrite grains can display large local variability in $\delta^{34}S$, with a range of up to 35‰ reported from pyrite grains within a single sediment sample (Kohn et al., 1998). It is therefore difficult to define a global average value for $\delta^{34}S_{pyr}$ from direct measurements. The $\delta^{34}S$ of marine pyrite is often taken to be between 15‰ and −50‰ (Strauss, 1997).

The other primary control on the $\delta^{34}S$ of marine sulfate is the flux of pyrite burial, which is often considered as the proportion of the total sulfur flux from the oceans (Garrels and Lerman, 1981; Halevy et al., 2012; Holser et al., 1988). This proportional pyrite burial flux varies with the availability of suitable environments for sulfate reduction, favored by anoxia either in the water column or in shallow organic-rich sediments, and the rate of active iron delivery (to precipitate the sulfide as pyrite). Assuming a $\delta^{34}S$ of river input and average $\delta^{34}S$ of pyrite buried, the $\delta^{34}S$ of marine sulfate has been used to place constraints on this proportional pyrite burial flux over time. Canfield (2004) argued that nearly all sulfur was buried as pyrite in the Precambrian and that the proportional fraction of pyrite burial dropped significantly during the Palaeozoic to around 30% today. A number of other studies have also suggested that the present-day proportional pyrite burial flux is close to 30–40% of the total sulfur lost from the oceans (Berner, 1989, 1987; Canfield, 2004; Kampschulte and Strauss, 2004; Kump and Garrels, 1986; Ono et al., 2006), with the rest of the sulfur leaving the oceans as evaporite minerals or in hydrothermal systems. Recently, Halevy et al. (2012) suggested that the net evaporite burial flux is lower than the estimates used in some of these models, and arrived at significantly higher Phanerozoic proportional net pyrite burial fluxes (70–90%). These authors suggested that the $\delta^{34}S$ of modern river input is elevated in its $\delta^{34}S$ due to contributions from rapidly recycled evaporites, and that when this 'gross flux' of evaporites is removed, the $\delta^{34}S$ of river input is lower and thus the proportional net pyrite burial flux must be much higher. Canfield (2013) has since shown that the $\delta^{34}S$ of Phanerozoic coal can be used to constrain the $\delta^{34}S$ of riverine input, and suggests that river input remained elevated throughout the Phanerozoic, indicating that the effect of these rapidly recycled evaporites has been present over the last 500 million years. The $\delta^{34}S$ of marine sulfate reflects the integrated riverine flux from both the rapidly recycled evaporites as well as the longer tectonically controlled weathering of ancient evaporites, pyrite and magmatic sulfide.

Inclusion of minor sulfur isotope ratios (e.g. $^{33}S/^{32}S$) may place additional constraints on the fraction of sulfur buried as pyrite (Ono et al., 2006) and also on biological reactions that partition, or separate, isotopes as a function of their mass (Johnston et al., 2005, 2006, 2008; Leavitt et al., 2013; C. Li et al., 2010; X. Li et al., 2010; Sim et al., 2011; Wu et al., 2010; Zerkle et al., 2009). If all sulfur isotope fractionation followed the same mass law, then the amount of ^{33}S in the modern ocean could be directly calculated from the relative amount of ^{34}S versus ^{32}S, and so no new information would be gained by measuring the less abundant sulfur isotopes. However, there are unique mass laws that control different mass dependent processes, and these can be identified using high-precision measurements of both major and minor sulfur isotopes. Deviations from expected mass dependence are reported using $\Delta^{33}S$ (Farquhar et al., 2000; Hulston and Thode, 1965; Ono et al., 2006), which is defined as:

$$\Delta^{33}S = \delta^{33}S - 1000\left[\left(1 + \frac{\delta^{34}S}{1000}\right)^{0.515} - 1\right] \quad (1)$$

where the reference mass dependence law has been assigned an exponent of 0.515. Small shifts from the theoretical equilibrium value of 0.515 occur in different metabolic pathways, and can generate small non-zero $\Delta^{33}S$ values on the order of a few tenths of a permil during purely mass-dependent biological processes. These deviations result from intracellular branching reactions with back-and-forth exchange of sulfur between multiple reservoirs (Farquhar et al., 2003, 2007; Johnston et al., 2005; Ono et al., 2006). These small variations in the exponent of Eq. (1) that are provided by the analysis of both $\delta^{33}S$ and $\delta^{34}S$ can be used to trace microbial processes in the sulfur cycle. Although the $\delta^{34}S$ of modern marine sulfate is well constrained, $\delta^{33}S$ has seldom been measured alongside $\delta^{34}S$. Some $\delta^{33}S$ data has been reported for standard materials that derive from seawater sulfate, IAEA-S2 and NBS-127 (Ono et al., 2006; Peters et al., 2010; Wu et al., 2010), as well as for several seawater samples from sites close to both Bermuda and Hawaii (Ono et al., 2012).

Sulfate reducing bacteria, sulfur disproportionating bacteria and sulfide oxidizing bacteria have all been assessed for their associated multiple sulfur isotope fractionations (Farquhar et al., 2003; Johnston et al., 2005, 2007; Zerkle et al., 2009). The minor isotope relationship describing the metabolism-specific effects or mass law is often expressed as $^{33}\lambda$. This term defines the slope a line in $\delta^{34}S$–$\delta^{33}S$ space and is defined as:

$$^{33}\lambda_{pyr-SW} = \frac{[\ln(1 + \frac{\delta^{33}S_{pyr}}{1000}) - \ln(1 + \frac{\delta^{33}S_{sw}}{1000})]}{[\ln(1 + \frac{\delta^{34}S_{pyr}}{1000}) - \ln(1 + \frac{\delta^{34}S_{sw}}{1000})]} \quad (2)$$

The $^{33}\lambda$ values measured for modern microbial communities range from 0.508 to 0.514 for sulfate reduction, with higher values describing oxidative metabolisms. Much work is needed to define the full range of fractionations and $^{33}\lambda$ that are possible during sulfur transformations, such as thermochemical sulfate reduction and inorganic sulfur oxidation. However, the values for sulfate reduction capture the geological average for all published sulfide data, suggesting that sulfate reducers are the primary sulfur isotope fractionation mechanism within the sulfur cycle (Johnston, 2011).

In this study we have measured both $\delta^{34}S$ and $\delta^{33}S$ in sulfate in modern seawater from sites at various locations and depths on the eastern margin of the Pacific Ocean, which we use to calculate the $\Delta^{33}S$ of marine sulfate. We use the average $\delta^{34}S$ and $\delta^{33}S$ of sulfate to build a box model to explore the range of possible $\delta^{34}S$ and $\delta^{33}S$ values associated with pyrite burial in modern marine sediments and then compare these with published pyrite sulfur isotope data. This is a methodologically different approach than has been taken previously. Constraints on $^{33}\lambda$ and the multiple sulfur isotope composition of riverine sulfur input are used to quantify the proportional flux of buried pyrite in modern ocean sediments.

2. Methods

Seawater samples were collected during two separate cruises to the eastern margin of the Pacific Ocean (Fig. 1). Samples from off the coast of Peru were collected in October–November 2005 through the Woods Hole Oceanographic Institute. These samples were collected between 0 and 3000 m depth, using Niskin bottles and then transferred into 60 mL HDPE bottles. The bottles were rinsed three times with sample prior to filling and stored frozen at −20 °C until analysis. Samples from off the coast of southern California were collected in June 2007. These samples were collected between 0 and 1000 m water depth using rosette mounted 10 L PVC Niskin Bottles in the San Clemente Basin. All samples were syringe filtered and stored without acid prior to isotope analyses.
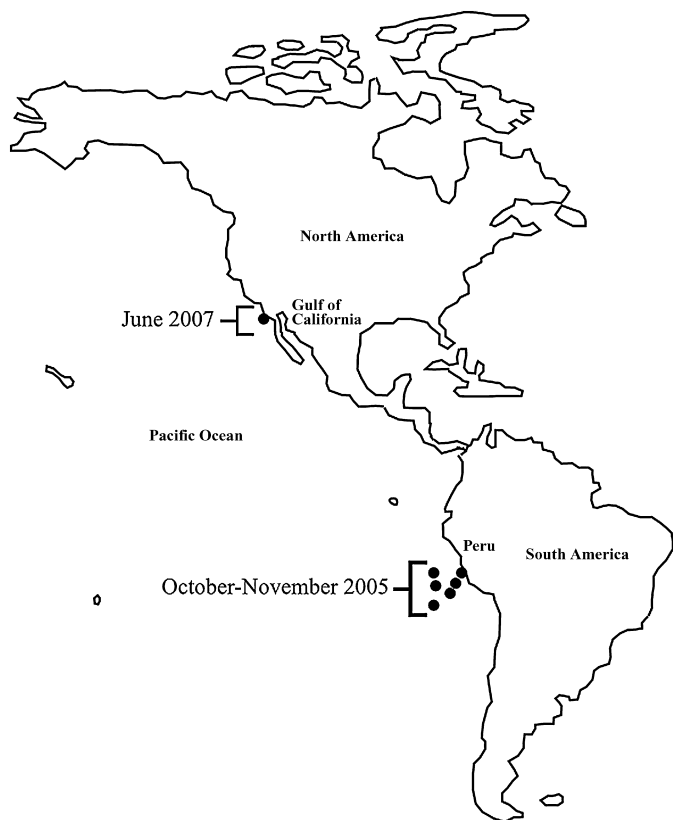
Fig. 1. Sampling locations along the eastern margin of the Pacific Ocean.

Table 1
The δ^{33}S, δ^{34}S and Δ^{33}S measured for sulfate from the open ocean, from a range of sites around the eastern margin of the Pacific Ocean.

Sample number	δ^{33}S	δ^{34}S	Δ^{33}S
1	11.22	21.81	0.046
2	10.39	20.17	0.052
3	10.96	21.29	0.045
4	11.01	21.38	0.052
5	10.94	21.26	0.045
6	10.92	21.21	0.051
7	11.09	21.53	0.058
8	10.84	21.04	0.060
9	10.93	21.22	0.057
10	10.87	21.11	0.047
11	11.13	21.62	0.053
12	10.83	21.02	0.054
13	11.12	21.58	0.064
14	11.35	22.05	0.053
15	10.86	21.12	0.033
16	11.04	21.45	0.044
17	11.19	21.73	0.055
18	11.37	22.10	0.044
19	10.53	20.46	0.045
20	10.86	21.08	0.055
21	10.53	20.42	0.061
22	11.00	21.37	0.050
23	10.92	21.20	0.054
24	10.84	21.06	0.050
25	10.82	21.00	0.054
26	10.85	21.10	0.039
27	11.01	21.39	0.052
28	10.83	21.06	0.036
Average	**10.94**	**21.24**	**0.050**
Standard deviation	0.22	0.44	0.007

Barite was precipitated from seawater sulfate using an excess of Barium Chloride. Samples of barite were reduced to H_2S gas by reaction with Thode reduction solution (Thode et al., 1961), heated to just below the boiling point and bubbled with nitrogen gas. The H_2S carried in nitrogen was then precipitated as silver sulfide using a silver nitrate trapping solution. Silver sulfide was aged for one week in the dark, washed with rinses of Milli-Q water and ammonium hydroxide, and then dried in an 80 °C oven. Approximately 2–4 mg of silver sulfide were weighed into an aluminum foil packet that was then placed in a nickel reaction vessel for fluorination. Fluorination was undertaken at 250 °C with 10 times excess fluorine gas to produce SF_6 gas, which was purified before being measured on a dual-inlet MAT 253 isotope ratio mass spectrometer. The method has been described in detail by Hu et al. (2003), Rumble et al. (1993) and Ono et al. (2006). All Δ^{33}S presented here are normalized to a composition for the international standard (IAEA S1) relative to V-CDT, of δ^{34}S $= -0.30$‰ and Δ^{33}S $= 0.107$‰.

3. Results

Sulfur isotope data are presented for sulfate from the modern open ocean from 28 samples from the eastern margin of the Pacific basin in Table 1. The δ^{34}S measures between 20.17‰ and 22.10‰, with an average of 21.24‰. We have taken our average δ^{34}S of 21.24‰, measured using the SF_6 technique, as the accepted seawater value in this study. The Δ^{33}S values for measured sulfate samples is positive, ranging from 0.033‰ to 0.064‰, with an average of 0.050‰. This value is consistent with previous data reported for sulfate derived from oceanic sulfate – reported via analyses of NBS-127 and IAEA-S2 – (e.g., Ono et al., 2006; Peters et al., 2010; Wu et al., 2010) as well as for independently collected seawater samples (Ono et al., 2012). Note that the values of Peters et al. (2010) and Wu et al. (2010) are reported assuming

IAEA S-1 has a different value, but when renormalized, match the measured value within uncertainty.

The standard deviation of the 28 seawater sulfate samples reported here is ± 0.88 and ± 0.014 (2σ) for δ^{34}S and Δ^{33}S. This error is large for δ^{34}S and comparable for Δ^{33}S to the long-term reproducibility for analyses of laboratory reference silver sulfide, ± 0.20 and ± 0.016 (2σ) for δ^{34}S and Δ^{33}S, measured at the University of Maryland. The larger uncertainty for δ^{34}S most likely reflects analytical issues associated with conversion of sulfate to silver sulfide using the Thode solution, as errors for laboratory reference silver sulfide only account for uncertainty associated with the fluorination process.

4. Model of the modern marine sulfur cycle

We used a steady-state isotope box model for the sulfur cycle in the modern ocean, using a range of accepted estimates of the input and output fluxes and their respective isotopic compositions (Table 2, Fig. 2) (Berner, 1987; Canfield, 2004; Garrels and Lerman, 1981; Holser et al., 1988; Ono et al., 2006). The model equations are derived from a standard one-box model for the ocean, whereby the change in the concentration and isotope composition of sulfate (which is zero at steady state) is a function of the sources and sinks of sulfate to the ocean and their respective isotope compositions. We invert this to solve for the sulfur isotope composition of pyrite. The governing model equations are:

$$\delta^{34}_{pyr} = \delta^{34}_{sw} - \varepsilon^{34}S_{sw\text{-}pyr}$$

$$= \delta^{34}_{sw} - \left[\left(\frac{-1}{F_{pyr}} \right) \cdot \left[F_{riv}\delta^{34}_{riv} - F_{pyr}\delta^{34}_{sw} \right. \right.$$

$$\left. \left. - F_{evap}\delta^{34}_{sw} - F_{hyd}\delta^{34}_{sw} \right] \right] \quad (3)$$

Table 2
Fluxes and multiple sulfur isotope compositions of the sources and sinks in our model of the modern sulfur cycle. Values in bold against a grey background have been measured, and values in white against a black background are calculated from the model. Values in italics are the result of constraints imposed on the model from the literature (e.g. $\delta^{34}S_{riv}$ between 0‰ and 16‰ (Berner and Canfield, 1989; Canfield, 2013; Garrels and Lerman, 1981), and $^{33}\lambda$ of between 0.508 and 0.514 (Johnston, 2011)). Other values result from assumptions we make about the modern marine sulfur cycle, as discussed in Section 4.

|	Flux	$\delta^{34}S$ (‰)	$\delta^{33}S$ (‰)	$\Delta^{33}S$ (‰)
Seawater		**21.24**	**10.94**	**0.050**
Input	$3E+12$ mol yr^{-1}	$\delta^{34}S$ must be between 0–16‰		
Evaporites	*20–80% of input flux*	21.24	10.94	0.050
Sedimentary sulfide	*10–30% of input flux*	−39.56	−20.43	0.144
Volcanic sulfide	*10–70% of input flux*	2	1.04	0.013
Output	*= input (mass steady state)*	= input (isotopic steady state)		
Evaporites	*10–80% of burial flux*	21.24	10.94	0.050
Hydrothermal	*10–80% of burial flux*	21.24	10.94	0.050
Pyrite	*10–45% of burial flux*	−69: −27	−35: −14	0.09: 0.60
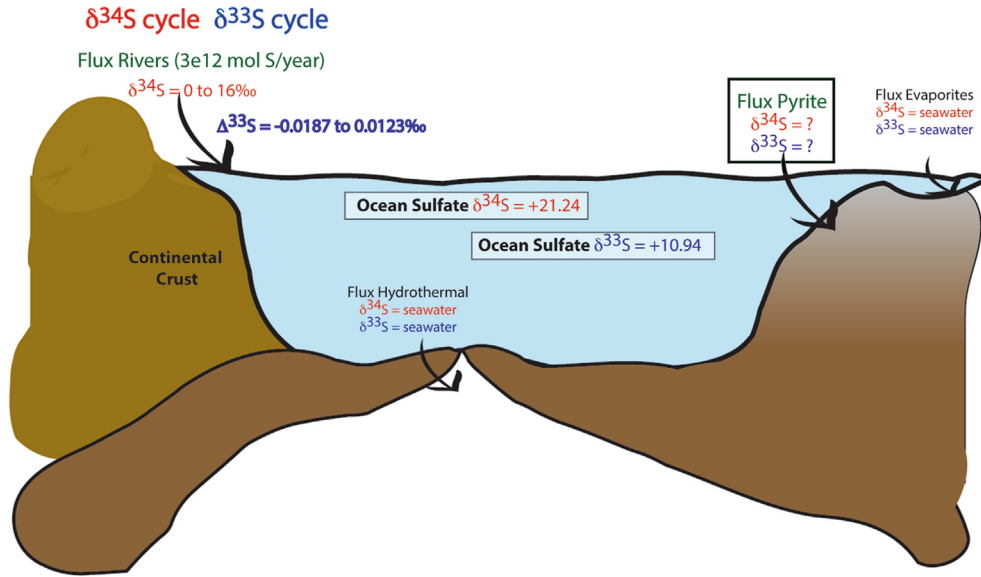
Fig. 2. Schematic diagrams of the input and output fluxes of sulfur to the modern ocean used to model the ^{33}S and ^{34}S cycles.

$$\delta^{33}_{pyr} = \delta^{33}_{sw} - \varepsilon^{33}S_{sw\text{-}pyr}$$

$$= \delta^{33}_{sw} - \left[\left(\frac{-1}{F_{pyr}} \right) \cdot \left[F_{riv}\delta^{33}_{riv} - F_{pyr}\delta^{33}_{sw} \right. \right.$$

$$\left. \left. - F_{evap}\delta^{33}_{sw} - F_{hyd}\delta^{33}_{sw} \right] \right] \quad (4)$$

Here F refers to flux of ^{32}S (in Mol yr^{-1}) of rivers (riv), pyrite burial (pyr), evaporite burial (evap), and hydrothermal burial (hyd). The δ in Eqs. (3) and (4) refer to the δ^{34}S (Eq. (3)) and δ^{33}S (Eq. (4)) isotope composition of the various fluxes. The ε in Eqs. (3) and (4) refers to the difference in δ values between seawater and pyrite.

With the isotopic composition of the modern ocean (21.24‰ and 0.050‰), these equations can be used to calculate a field of possible values for the average δ^{34}S–Δ^{33}S of pyrite being buried today (Table 2 and Fig. 3). The validity of this treatment hinges on three key assumptions:

1) that removal of sulfur in hydrothermal systems and evaporite basins is quantitative,
2) the value of average global δ^{34}S and Δ^{33}S of the riverine sulfate input, and
3) that the sulfur cycle is presently in a numerical steady state.

In hydrothermal systems, ridge flank fluids frequently have sulfate concentrations much lower than seawater, indicating a net loss of sulfur during fluid flow through the crust. However, the cycling of sulfur in hydrothermal systems is complex (Hansen and Wallmann, 2003), with addition of sulfur from igneous sulfide minerals and removal of sulfur through the formation of anhydrite, sulfate reduction and alteration of the ocean crust (Alt et al., 2012). Mass balance of sulfur isotopes at hydrothermal vents suggests that the majority of sulfur in hydrothermal fluid is mantle derived with very small fraction from seawater sulfate. Anhydrite precipitated at high temperatures may be released back into seawater as the crust cools and moves away from the ridge, meaning this process may not act as a significant long-term net sink for sulfur (Alt, 1995). Where temperatures are too low for hydrothermal anhydrite formation, sulphate may primarily be lost through sulfate reduction and subsequent pyrite precipitation. The sulfur isotope fractionation during sulfate reduction in the subseafloor may be quite large (Shanks et al., 1981; Shanks and Seyfried, 1987), however this sink would be included in our model, which reflects global pyrite formation regardless of the sediment or rock type. Therefore the net flux of sulfur that is lost (or gained) from (or to) the ocean in hydrothermal systems is not well constrained, but is considered small compared with the loss through evaporite or pyrite formation (Alt et al., 2013). We assume that any sulfur isotope fractionation that occurs during net
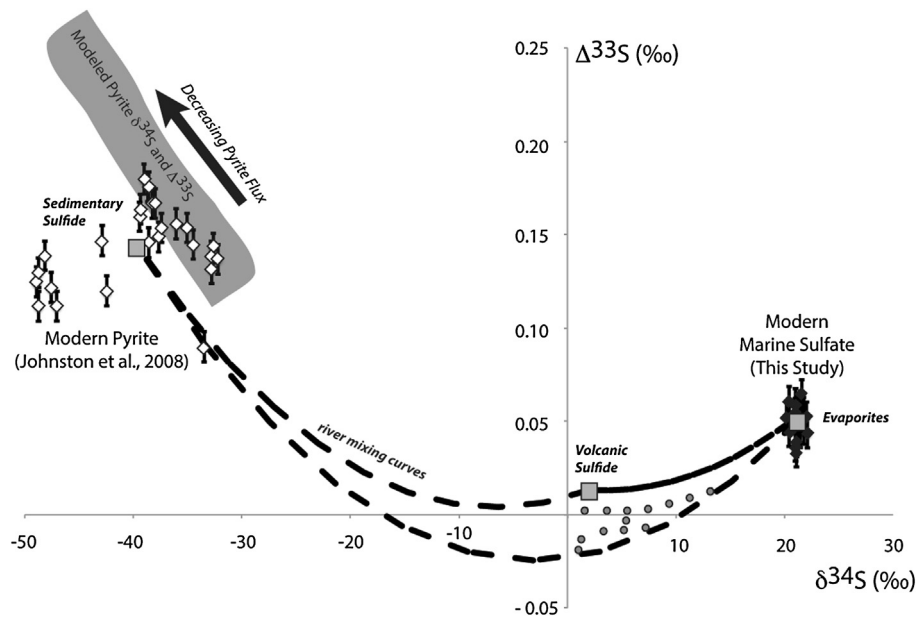
Fig. 3. Calculated range of possible $\delta^{34}S$ and $\Delta^{33}S$ for the modern pyrite sink for a range of riverine $\delta^{34}S$ and $\Delta^{33}S$ and a varying pyrite burial flux (grey box) and measured $\delta^{34}S$ and $\Delta^{33}S$ data for sulfate in the modern open ocean (black diamonds). Modern pyrite data from Johnston et al. (2008) is plotted for comparison (open diamonds). Also shown are the accepted $\delta^{34}S$ and $\Delta^{33}S$ values for the three mineralogical sources that combine to produce the average weathered riverine sulfur input (grey squares), and the mixing curves for two component mixing of each of these sources (dashed lines). The small grey circles are the result of mixing all three riverine source areas in combinations that produce a $\delta^{34}S_{riv}$ between 0 and 16‰.

removal of sulfate at hydrothermal vents is small, and that the bulk sink can be considered quantitative.

Evaporite formation is likely a major pathway for sulfur removal from the ocean over geological timescales. During evaporite formation, sulfate is removed as gypsum, $CaSO_4*2H_2O$. In the modern ocean, sulfate (28 mM) is in excess relative to calcium (10 mM), but other sulfate salts likely make up the difference during quantitative evaporation (Spencer, 2000). However, removal rates of evaporite minerals are not time-steady, and are dependent on the global availability of sites suitable for seawater evaporation, such as partially enclosed basins, the availability of which is often controlled tectonically. Our flux is therefore time-integrated for the past 20 Myr (the approximate residence time of sulfur in the ocean). A large fraction of the evaporite flux is likely to be made up of recently deposited and rapidly recycled evaporites, as discussed in the introduction (Halevy et al., 2012). Sulfur isotope fractionation during evaporite formation has been shown to be minimal, up to +2.4‰ (Raab and Spiro, 1991; Thode et al., 1961). Although no measurements exist for $\Delta^{33}S$ partitioning during evaporite formation, we know of no pathway for significant deviations from the equilibrium sulfur isotope fractionation to occur during this abiotic process, and thus assume both $\delta^{34}S$ and $\Delta^{33}S$ of evaporites is equivalent to seawater.

We have tested the sensitivity of our model to these assumptions by altering the $\Delta^{33}S$ value associated with the hydrothermal and evaporite sink between 0.025 and 0.075 (around the initial value of $0.050 = SW$). This does not affect the resulting pyrite burial flux solutions by more than three percent. The model is therefore not particularly sensitive to this assumption, and both removal fluxes have been assigned an isotope composition equal to the isotope composition of the ocean ($\delta^{34}S_{SW}$ and $\delta^{33}S_{SW}$).

The modern riverine sulfur flux is often assigned a $\delta^{34}S$ of +8‰, but the true composition of globally averaged riverine sulfate remains enigmatic (Canfield, 2004, 2013; Holser et al., 1988; Kurtz et al., 2003). We therefore use our model to explore the range of $\delta^{34}S$ and $\Delta^{33}S$ (and thus $\delta^{33}S$) of riverine input. There are three isotopically distinct mineralogical sources for riverine sulfur: evaporite minerals, sedimentary sulfide (e.g. pyrite), and volcanic

sulfide. The average sulfur isotope composition of weathered evaporite minerals reflects that of its seawater source at the time of precipitation. It has been suggested that as much as half the modern riverine sulfate flux comes from weathering of recently deposited evaporites (Halevy et al., 2012), leaving this flux with a sulfate isotopic composition closer to the modern ocean (Paytan et al., 1998). Sulfur isotope analyses of coal over the Phanerozoic suggest that rivers have been similarly elevated towards seawater values for the last 500 million years (Canfield, 2013). We use this presumption and set the sulfur isotope composition of the evaporite end-member for weathering at 21.24‰ ($\delta^{34}S$) and 0.050‰ ($\Delta^{33}S$). We assign sedimentary sulfides a negative $\delta^{34}S$ of $-39.56‰$, and a higher $\Delta^{33}S$ of 0.142‰, values that reflect the average composition of pyrite buried in the ocean over the recent past (values are from pyrite formed in normal marine and euxinic modern environments, reported by Johnston et al., 2008). Igneous sulfide is taken to have a $\delta^{34}S$ of +2‰, and $\Delta^{33}S$ of 0.013, approximating the bulk Earth. The oxidative weathering of volcanic sulfide is thought to have a similar sulfur isotope composition to igneous sulfides (Canfield, 2004; Garrels and Lerman, 1984; Halevy et al., 2012). Given these isotopic end-members for possible sources of riverine sulfate, we calculate the range of possible $\delta^{34}S$ and $\Delta^{33}S$ of rivers resulting from a range of different proportional contributions, with the one constraint being that each of the three sources made up a minimum of 10% of the total flux (Fig. 3 and Table 2). This results in a wide range of possible $\delta^{34}S_{riv}$. We further limit the possible combination of riverine sources to only allow weathering scenarios that produce a $\delta^{34}S_{riv}$ between 0‰ and +16‰, around the 'accepted' value of 8‰, and inclusive of the range of reported $\delta^{34}S_{riv}$ in the literature. This results in a range of $\delta^{34}S$ of river inputs that have an independent, but associated, $\Delta^{33}S$ value, which is used to calculate the relative ^{33}S flux into the ocean.

For each combination of possible $\delta^{34}S$ and $\delta^{33}S$ values of riverine sulfur input, we calculate the $\delta^{34}S$ and $\delta^{33}S$ of pyrite burial across a range of possible pyrite burial fluxes. We varied the relative proportion of the total flux that is removed through each of the three defined sinks from 90% pyrite burial to 5% pyrite burial,

with the remaining sink split between hydrothermal and evaporite burial, which we have assumed to be isotopically equivalent to one another and to seawater. We use the calculated δ^{34}S and δ^{33}S of pyrite burial to calculate a Δ^{33}S value for pyrite burial using Eq. (1). This multiple sulfur isotope composition of pyrite yields information about the isotope partitioning during sulfate reduction and a corresponding $^{33}\lambda$ value for sulfate reduction.

This provides us with a range of potential sulfur isotopic compositions for pyrite buried in the modern ocean, which we further constrain by neglecting those that are associated with $^{33}\lambda$ values for sulfate reduction outside of the expected range for biological processes: 0.508 and 0.514 (Johnston, 2011). These endmember values for $^{33}\lambda$ come from experimental work on pure cultures, described in Section 1. In natural environments, the complexity of the sedimentary sulfur cycle may introduce sulfur isotope fractionations that are unlike those observed in pure culture. The range of sulfur isotope fractionation during microbial sulfate reduction measured in pure culture and in natural environments were thought to be significantly different, but more recent work has closed this gap (Canfield et al., 2010; Leavitt et al., 2013; Sim et al., 2011). Further work is needed to develop a thorough diagenetic model that includes minor sulfur isotopes before we can account for possible effects of advection, diffusion and reoxidation on the $^{33}\lambda$ in the natural environment. In the absence of comprehensive measurements from natural environments, experimental limits on $^{33}\lambda$ should provide reasonable boundaries for processes in modern marine sediments. Our model also relies on the assumption that sulfate reduction is the dominant process in modern ocean sediments (Leavitt et al., 2013), although other processes such as abiotic sulfate reduction, microbial sulfur disproportionation and sulfide oxidation may make a minor contribution to resulting overall sulfur isotope fractionations. However, it is unlikely that including these processes would result in $^{33}\lambda$ outside the stated range of 0.508–0.514 (Johnston et al., 2006; C. Li et al., 2010; X. Li et al., 2010; Zerkle et al., 2010). This assumption is supported by geological compilations that show the net multiple sulfur isotope signal for modern pyrite is close to the range produced by sulfate reducing microbes. The calculations for the sulfur isotope composition of pyrite are given in Table 2. These calculated pyrite sulfur isotope compositions are plotted alongside our measured δ^{34}S and Δ^{33}S in Fig. 3. We define fractional pyrite burial as:

$$f_{pyr} = F_{pyr}/F_{riv} \qquad (5)$$

Only f_{pyr} solutions between 8.5% and 44% satisfy mass and isotope steady state as well as our assumptions about riverine δ^{34}S and the biological constraints on $^{33}\lambda$. Additionally, we define a more likely range of constraints on f_{pyr}, using new data to constrain $\delta^{34}S_{riv}$ to between 3 and 8‰ (Canfield, 2013), and $^{33}\lambda$ endmembers that fall close to the mean of all measurements of $^{33}\lambda$ in biological cultures (0.5125–0.5135). We repeat our calculations using these tighter constraints, and this gives more likely f_{pyr} solutions of between 22% and 36% (Fig. 4). These solutions are consistent with previous work that considered ^{33}S, giving f_{pyr} solutions between 17 and 26% (Ono et al., 2006).

5. Discussion

Our study presents new data that constrains the multiple sulfur isotope composition of modern marine sulfate. Although several past studies have measured δ^{34}S of modern marine sulfate and established that it is broadly homogeneous throughout the ocean, there is less data for $\Delta^{33}S_{SO_4}$. The Δ^{33}S value we have measured is homogeneous within error and of the magnitude anticipated given fractionation during sulfur cycling in modern microbial communities. Ono et al. (2012) presented six measurements of δ^{34}S and Δ^{33}S from Hawaii and Bermuda at various depths, and noted their average values of 21.3‰ and 0.050‰ respectively, consistent with values presented here.

δ^{34}S and Δ^{33}S measurements made on sedimentary pyrite from a range of modern environments show a large spread of sulfur isotope compositions (shown on Fig. 3) (Johnston et al., 2008), reflecting the many variables that control sulfur isotope fractionation during sulfide, and therefore pyrite production. By comparing δ^{34}S and Δ^{33}S measured on modern pyrite with the δ^{34}S and Δ^{33}S predicted from our model, it may be possible to better constrain the sulfur isotope fractionation associated with pyrite burial today. The intersection between these data for modern pyrite and our calculations suggests that the composition of globally averaged buried pyrite is approximately -35 ± 5‰ (δ^{34}S) and 0.145 ± 0.025‰ (Δ^{33}S). Calculated Δ^{33}S values show the closest overlap with measured data when pyrite burial fluxes are higher, between 30% and 45%. Our calculated sulfur isotope composition of marine pyrite is more ^{34}S-depleted than estimated by Wu et al. (2010), in part because they infer a lower Δ^{33}S and less negative δ^{34}S composition for weathered pyrite than that used in our riverine input model. In addition, there may be a slight bias towards more positive δ^{34}S in the Wu et al. (2010) sulfide data compilation, which will improve as more data is collected. However, there is a good match between the two studies, given the uncertainties involved and the different methods employed.

Past studies that have quantified the global pyrite burial flux using δ^{34}S measurements alone yield estimates for f_{pyr} in the modern ocean from 10% to 90% of the total riverine input (Canfield, 2004; Canfield and Farquhar, 2009; Halevy et al., 2012; Kampschulte and Strauss, 2004). We suggest here that f_{pyr} between around 10% and 45% is consistent with our measured ocean δ^{33}S values, and that a narrower range of endmembers for the δ^{34}S of riverine input (3–8‰) and lambda values produced during sulfate reduction (0.5125–0.5135), results in a 'more likely' f_{pyr} of between around 20% and 35% (Fig. 4). The fractional pyrite burial flux depends critically on the sulfur isotopic composition of river input: the larger the contribution from the weathering of evaporites, the lower the fractional pyrite burial to maintain the same sulfur isotope composition of the ocean. For example, our model suggests that if evaporites contribute 80% of the global total sulfur delivery to rivers then pyrite burial could be as low as 10% of the marine sulfur sink in steady state. Thus deconvolving the river flux into its various components becomes critical for evaluating the relative fluxes in the sulfur cycle.

This deconvolution was recently done by Halevy et al. (2012), who separated the riverine sulfur flux into sulfur sourced from old rocks (ancient evaporites and sedimentary pyrites), and sulfur sourced from young evaporites with a sulfur isotope composition similar to modern seawater. Halevy et al. (2012) were able to do this deconvolution using North American/Caribbean derived macro-stratigraphic records, which record only long-term evaporite burial. Halevy et al. (2012) suggested that the measurements of modern riverine δ^{34}S are artificially biased towards an evaporite end member due to the weathering of recently deposited evaporites, which may contribute up to 50% of the riverine weathering flux. This means that using the riverine δ^{34}S of 5 to 15‰ biases all models of the marine sulfur cycle towards lower fractional pyrite burial fluxes, similar to our model results. We base our calculations on the modern ocean sulfur isotope composition, which includes the river flux comprised of both weathering of rapidly recycled evaporites as well as weathering of ancient evaporites, sedimentary sulfides, and volcanic sulfides. If we redo our calculations and include a rapidly recycled evaporite flux of 50% of riverine input, the resulting f_{pyr} of 40–70% is more consistent with the Halevy et al. (2012) range of 70–90%.
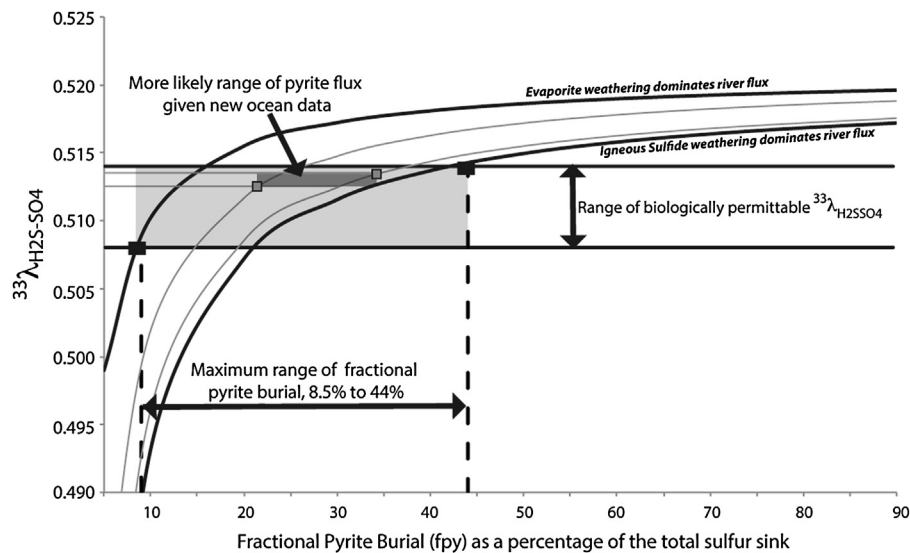
Fig. 4. $^{33}\lambda$ values that would be produced during sulfate reduction for a given riverine $\delta^{34}S$ and $\Delta^{33}S$ input across a range of f_{pyr}. Riverine fluxes with a $\delta^{34}S$ between 0 and 16‰ (black curves) intersect the upper and lower bounds for $^{33}\lambda$ (black lines), constraining the plausible range of results to f_{pyr} between 8.5% and 44% (light grey box). The range of f_{pyr} that could result from tighter constraints on $\delta^{34}S_{riv}$ (grey curves) and $^{33}\lambda$ (grey lines) are highlighted by the dark grey box, giving a range of 22% to 36% for f_{pyr}.

The consistency between our calculated pyrite burial flux and previous work is particularly encouraging because our model uses a variant of the approach used in other studies seeking to constrain f_{pyr}. The work described herein draws on constraints from isotopic balance rather than on inferences about the fractionation associated with sulfate reduction and pyrite formation, as was done elsewhere (Ono et al., 2006; Wu et al., 2010). Our model does still rely on some of the same assumptions that limited previous models, such as the quantitative nature of the evaporite and hydrothermal sinks, and introduces the further assumption that these sinks also have a zero $\Delta^{33}S$ value. The main strength of our model is that it is not directly reliant on the value of $\delta^{34}S_{pyr}$, or the fractionation associated with sulfate reduction and pyrite formation, both of which are difficult to independently constrain. Although this assumption is still necessary to model the riverine flux within our model, the impact of the uncertainty is greatly reduced.

Pyrite burial is one of the major pathways by which sulfur is lost from the oceans, and the magnitude of the flux will have a governing effect on the pH of seawater, since sulfur is an important component of the marine alkalinity budget (Morel et al., 1993). The process of sulfide production through microbial sulfate reduction also accounts for around half of organic matter respiration in marine sediments, and so is essential for balancing the organic carbon cycle (Jørgensen, 1982). Tighter constraints on the production of pyrite in today's ocean, provided by our model, are key to our understanding of these important biogeochemical processes.

Because the reduction of sulfate and burial of sulfide leaves oxidized products in the surface environment, pyrite is considered a major indirect source of oxygen to the atmosphere (Berner, 1987; Canfield, 2005). It has been suggested that major fluctuations in atmospheric oxygen, partially controlled by changes in pyrite burial fluxes, may influence major evolutionary events such as animal radiations and mass extinctions (Canfield et al., 2007; Fike et al., 2006). Our new method, here applied to modern environments, could be the first step towards improving constraints on the pyrite burial flux in deep time.

6. Conclusions

We report measurements of ^{32}S, ^{33}S and ^{34}S for 28 sulfate samples from a range of water depths along the eastern margin

of the Pacific Ocean. Using assumptions about the sulfur isotopic composition of riverine sulfur from the mixing of three separate reservoirs, we could constrain the range of sulfur isotopic compositions expected for pyrite burial in the modern ocean. The inclusion of ^{33}S measurements alongside ^{34}S and ^{32}S allowed us to reduce uncertainty in estimates of fluxes in the sulfur cycle by calculating the exponent involved in sulfate reduction to sulfide (preserved as pyrite) in modern marine sediments. We use assumptions about riverine input, combined with new analyses of multiple sulfur isotopes in marine sulfate, to estimate that the pyrite burial flux in the modern ocean is between around 10% and 45% of the total sulfur burial flux, with a more likely range of between around 20% and 35%.

Acknowledgements

References

Alt, J.C., 1995. Sulfur isotopic profile through the oceanic crust: sulfur mobility and seawater–crustal sulfur exchange during hydrothermal alteration. Geology 23 (7), 585–588.

Alt, J.C., et al., 2012. Uptake of carbon and sulfur during seafloor serpentinization and the effects of subduction metamorphism in Ligurian peridotites. Chem. Geol. 322–323, 268–277.

Alt, J.C., et al., 2013. The role of serpentinites in cycling of carbon and sulfur: seafloor serpentinization and subduction metamorphism. Lithos 178, 40–54.

Berner, Robert A., 1987. Models for carbon and sulfur cycles and atmospheric oxygen; application to Paleozoic geologic history. Am. J. Sci. 287 (3), 177–196.

Berner, Robert A., 1989. Biogeochemical cycles of carbon and sulfur and their effect on atmospheric oxygen over phanerozoic time. Palaeogeogr. Palaeoclimatol. Palaeoecol. 75 (1–2), 97–122.

Berner, R.A., Canfield, D.E., 1989. A new model for atmospheric oxygen over Phanerozoic time. Am. J. Sci. 289 (4), 333–361.

Canfield, D.E., 2004. The evolution of the Earth surface sulfur reservoir. Am. J. Sci. 304 (10), 839–861.

Canfield, D.E., 2005. The early history of atmospheric oxygen: homage to Robert M. Garrels. Annu. Rev. Earth Planet. Sci. 33 (1), 1–36.

Canfield, Donald E., 2013. Sulfur isotopes in coal constrain the evolution of the Phanerozoic sulfur cycle. Proc. Natl. Acad. Sci. USA 110 (21), 8443–8446.

Canfield, Donald E., Farquhar, James, 2009. Animal evolution, bioturbation, and the sulfate concentration of the oceans. Proc. Natl. Acad. Sci. USA 106 (20), 8123–8127.

Canfield, Don E., Poulton, S.W., Narbonne, G.M., 2007. Late-Neoproterozoic deep-ocean oxygenation and the rise of animal life. Science 315 (5808), 92–95.

Canfield, Donald E., Farquhar, James, Zerkle, A.L., 2010. High isotope fractionations during sulfate reduction in a low-sulfate euxinic ocean analog. Geology 38 (5), 415–418.

Chambers, L.A., Trudinger, P.A., 1979. Microbiological fractionation of stable sulfur isotopes: a review and critique. Geomicrobiol. J. 1 (3), 249–293.

Farquhar, James, et al., 2000. Evidence of atmospheric sulphur in the martian regolith from sulphur isotopes in meteorites. Nature 404 (6773), 50–52.

Farquhar, James, et al., 2003. Multiple sulphur isotopic interpretations of biosynthetic pathways: implications for biological signatures in the sulphur isotope record. Geobiology 1 (1), 27–36.

Farquhar, James, et al., 2007. Isotopic evidence for Mesoarchaean anoxia and changing atmospheric sulphur chemistry. Nature 449 (7163), 706–709.

Fike, D.A., et al., 2006. Oxidation of the Ediacaran Ocean. Nature 444 (7120), 744–747.

Garrels, R.M., Lerman, A., 1981. Phanerozoic cycles of sedimentary carbon and sulfur. Proc. Natl. Acad. Sci. 78 (8), 4652–4656.

Garrels, R.M., Lerman, A., 1984. Coupling of the sedimentary sulfur and carbon cycles; an improved model. Am. J. Sci. 284 (9), 989–1007.

Halevy, I., Peters, S.E., Fischer, W.W., 2012. Sulfate burial constraints on the Phanerozoic sulfur cycle. Science 337 (6092), 331–334.

Hansen, K.W., Wallmann, K., 2003. Cretaceous and Cenozoic evolution of seawater composition, atmospheric O_2 and CO_2: a model perspective. Am. J. Sci. 303 (2), 94–148.

Holser, W., Schidlowski, M., Mackenzie, M., 1988. Geochemical cycles of carbon and sulfur. In: Chemical Cycles in the Evolution of the Earth, pp. 105–173.

Hu, G., Rumble, Douglas, Wang, P., 2003. An ultraviolet laser microprobe for the in situ analysis of multisulfur isotopes and its use in measuring Archean sulfur isotope mass-independent anomalies. Geochim. Cosmochim. Acta 67 (17), 3101–3118.

Hulston, J.R., Thode, H.G., 1965. Variations in the S33, S34, and S36 contents of meteorites and their relation to chemical and nuclear effects. J. Geophys. Res. 70 (14), 3475–3484.

Johnston, D.T., 2011. Multiple sulfur isotopes and the evolution of Earth's surface sulfur cycle. Earth-Sci. Rev. 106 (1–2), 161–183.

Johnston, D.T., et al., 2005. Multiple sulfur isotope fractionations in biological systems: a case study with sulfate reducers and sulfur disproportionators. Am. J. Sci. 305 (6–8), 645–660.

Johnston, David T., et al., 2006. Evolution of the oceanic sulfur cycle at the end of the Paleoproterozoic. Geochim. Cosmochim. Acta 70 (23), 5723–5739.

Johnston, D.T., Farquhar, James, Canfield, Donald E., 2007. Sulfur isotope insights into microbial sulfate reduction: when microbes meet models. Geochim. Cosmochim. Acta 71 (16), 3929–3947.

Johnston, D.T., et al., 2008. Sulphur isotopes and the search for life: strategies for identifying sulphur metabolisms in the rock record and beyond. Geobiology 6 (5), 425–435.

Jørgensen, B.B., 1982. Mineralization of organic matter in the sea bed – the role of sulphate reduction. Nature 296 (5858), 643–645.

Kampschulte, A., Strauss, H., 2004. The sulfur isotopic evolution of Phanerozoic seawater based on the analysis of structurally substituted sulfate in carbonates. Chem. Geol. 204 (3–4), 255–286.

Kaplan, Isaac R., 1983. Stable isotopes in sedimentary geology. In: Society for Sedimentary Geology Short Course Notes. Tulsa, OK, pp. 1–108.

Kaplan, I.R., Rittenberg, S.C., 1964. Microbiological fractionation of sulphur isotopes. J. Gen. Microbiol. 34 (2), 195–212.

Kohn, M.J., et al., 1998. Sulfur isotope variability in biogenic pyrite; reflections of heterogeneous bacterial colonization?. Am. Mineral. 83 (11–12 Part 2), 1454–1468.

Krouse, H.R., 1980. Sulfur Isotopes in Our Environments. Elsevier.

Kump, Lee R., Garrels, R.M., 1986. Modeling atmospheric O_2 in the global sedimentary redox cycle. Am. J. Sci. 286 (5), 337–360.

Kurtz, A.C., et al., 2003. Early Cenozoic decoupling of the global carbon and sulfur cycles. Paleoceanography 18 (4), 14.1–14.14.

Leavitt, W.D., et al., 2013. Influence of sulfate reduction rates on the Phanerozoic sulfur isotope record. Proc. Natl. Acad. Sci 110 (28), 11244–11249.

Li, C., et al., 2010. A stratified redox model for the Ediacaran ocean. Science 328 (5974), 80–83.

Li, X., et al., 2010. Stable sulfur isotopes in the water column of the Cariaco Basin. Geochim. Cosmochim. Acta 74 (23), 6764–6778.

Morel, F., Hering, J.G., Morel, F., 1993. Principles and applications of aquatic chemistry. Available at http://agris.fao.org/agris-search/search.do?f=2012/OV/OV201204395004395.xml. US19940060000 [Accessed 19 January 2014].

Ono, S., et al., 2006. Mass-dependent fractionation of quadruple stable sulfur isotope system as a new tracer of sulfur biogeochemical cycles. Geochim. Cosmochim. Acta 70 (9), 2238–2252.

Ono, S., et al., 2012. Sulfur-33 constraints on the origin of secondary pyrite in altered oceanic basement. Geochim. Cosmochim. Acta 87, 323–340.

Paytan, Adina, et al., 1998. Sulfur isotopic composition of Cenozoic seawater sulfate. Science 282 (5393), 1459–1462.

Paytan, Adina, et al., 2004. Seawater Sulfur Isotope Fluctuations in the Cretaceous. Science 304 (5677), 1663–1665.

Peters, M., et al., 2010. Sulfur cycling at the Mid-Atlantic Ridge: a multiple sulfur isotope approach. Chem. Geol. 269 (3–4), 180–196.

Raab, M., Spiro, B., 1991. Sulfur isotopic variations during seawater evaporation with fractional crystallization. In: Isotope Geoscience Section. Chem. Geol. 86 (4), 323–333.

Rees, C.E., 1978. Sulphur isotope measurements using SO_2 and SF_6. Geochim. Cosmochim. Acta 42 (4), 383–389.

Rumble, D., Hoering, T., Palin, J., 1993. Preparation of SF_6 for sulfur isotope analysis by laser heating sulfide minerals in the presence of F_2 gas. Geochim. Cosmochim. Acta 57 (18), 4499–4512.

Shanks III, W.C., Bischoff, J.L., Rosenbauer, R.J., 1981. Seawater sulfate reduction and sulfur isotope fractionation in basaltic systems: interaction of seawater with fayalite and magnetite at 200–350 °C. Geochim. Cosmochim. Acta 45 (11), 1977–1995.

Shanks, W.C., Seyfried, W.E., 1987. Stable isotope studies of vent fluids and chimney minerals, southern Juan de Fuca Ridge: sodium metasomatism and seawater sulfate reduction. J. Geophys. Res., Solid Earth 92 (B11), 11387–11399.

Sim, M.S., Bosak, T., Ono, S., 2011. Large sulfur isotope fractionation does not require disproportionation. Science 333 (6038), 74–77.

Spencer, R.J., 2000. Sulfate minerals in evaporite deposits. Rev. Mineral. Geochem. 40 (1), 173–192.

Strauss, H., 1997. The isotopic composition of sedimentary sulfur through time. Palaeogeogr. Palaeoclimatol. Palaeoecol. 132 (1–4), 97–118.

Thode, H., Monster, J., Dunford, H., 1961. Sulphur isotope geochemistry. Geochim. Cosmochim. Acta 25 (3), 159–174.

Wu, N., et al., 2010. Evaluating the S-isotope fractionation associated with Phanerozoic pyrite burial. Geochim. Cosmochim. Acta 74 (7), 2053–2071.

Zerkle, A.L., et al., 2009. Fractionation of multiple sulfur isotopes during phototrophic oxidation of sulfide and elemental sulfur by a green sulfur bacterium. Geochim. Cosmochim. Acta 73 (2), 291–306.

Zerkle, A.L., et al., 2010. Sulfur cycling in a stratified euxinic lake with moderately high sulfate: constraints from quadruple S isotopes. Geochim. Cosmochim. Acta 74 (17), 4953–4970.